Journal of Ceramic Processing Research. Vol. 26, No. 5, pp. 734~741 (2025)
(Received 8 July 2025, Received in revised form 9 September 2025, Accepted 10 September 2025)
https://doi.org/10.36410/jcpr.2025.26.5.734

J O U R N A L O F
Ceramic Processing Research

Identification of layer thickness and rheological properties of ceramic shell slurry of investment casting

Agus Edy Pramono[a,*], Arif Dermawan[b] and Nanik Indayaningsih[c]
[a]*Magister Program in Applied Manufacturing Technology Engineering, Politeknik Negeri Jakarta, Jln. Prof. Dr. G.A. Siwabessy, Kampus UI. Depok 16425, Jawa-Barat, Indonesia*
[b]*Department of Mechanical Engineering, Politeknik Negeri Jakarta Jln. Prof. Dr. G.A. Siwabessy, Kampus UI. Depok 16425, Jawa-Barat, Indonesia*
[c]*Research Centre for Physics, National Research and Innovation Agency (BRIN), Kawasan Puspiptek, Gd. 440-442, Tangerang Selatan, Banten 15310, Indonesia*

This study explores the rheological behavior of slurries and the distribution of elements within investment casting molds, based on microstructural analysis. The rheological characteristics of ceramic shell slurry used in investment casting are examined through its microstructure. The uneven surfaces of sand grains promote mechanical interlocking at grain boundaries, leading to effective agglomeration of ceramic shells ideal for investment casting applications. The shell mold examined comprises aggregates such as stucco sand, mullite, and colloidal silica, which serve as inorganic binders on fungal shells. The colloidal silica observable in the image represents the slurry's rheological flow post-sintering. Its mechanical binding capabilities are evidenced by its interaction with aggregates featuring irregular surface textures. Acting as a binding agent, the slurry enables the formation of consolidated ceramic molds. Slurry rheology is influenced by its viscosity and the shear rate during flow between the aggregates. These factors, in turn, affect the slurry's shear stress, which is governed by applied pressure and immersion depth. After sintering at 1050 °C, the ceramic shell displays its highest oxygen concentration, registering 56.11%, alongside silica at 20.91%, aluminum at 13.02%, and carbon at 9.10%.

Keywords: Rheology properties, Slurry shear stress, Slurry viscosity, Slurry shear rate, Investment casting.

Introduction

This paper reveals the rheological conditions of slurries and element distribution through microstructural observations on the investment casting molds of centrifugal pump impellers. This paper does not discuss the study of centrifugal pump impellers as a product example.

Investment casting is a method used to produce complex parts that cannot be fabricated by other means. This method can create components with accurate dimensions, ideal for manufacturing very thin-walled parts. These parts show a smooth final surface, eliminating the need for further finishing processes [1-4]. The use of protective coatings is crucial in thin-walled investment casting methods for manufacturing stents from magnesium alloys. Mold models coated with Y_2O_3 have a more homogeneous, clean, and well-defined microstructure, whereas models without the protective coating undergo damaging reactions and exhibit coarse microstructures [5]. In this study, the Wilhelmy and Du-Nuoy methods were used to measure the properties of the wax. The Du-Nuoy ring method is more practical and provides more consistent results. The use of a standard correction factor in the Wilhelmy method is not necessary because the reported difference in results is not significant [6]. Hot permeability and hot strength are two crucial properties in investment casting molds. In this study, a new method was developed to sequentially evaluate both properties. This method provides a more accurate understanding of mold performance at high temperatures [7].

The roughness of cast surfaces is influenced by the quality of the mold surface, molten metal, and foam patterns. The use of nitrocellulose coating on foam patterns reduces roughness to 0.87 μm and on the mold to 1-2 μm higher. The filler size in the surface layer affects the mold roughness, but once the mesh size reaches 200, the roughness remains around 2.4 μm. The selection of silica sol results in lower casting roughness compared to sodium silicate [8]. Porous mullite ceramics possess properties such as low thermal expansion coefficient, chemical durability, high mechanical strength, and deformation resistance. To enhance their porosity, pore-forming agents like cornstarch and graphite are used. Modified image analysis techniques can be utilized to

*Corresponding author:
Tel : +62217863530
Fax: +62217863530
E-mail: agus.edypramono@mesin.pnj.ac.id

evaluate the pore structure. This information is crucial for mullite membrane applications [9]. The microstructure shows increased sinter bonding and densification zones at 2150 °C. SiC is uniformly dispersed in B_4C, helping to inhibit the growth of B_4C grains. The strong B_4C/SiC interfacial bonding and the mechanisms of crack deflection and bridging in the SiC grains contribute to the reinforcement of the composite [10]. Shells with higher refractory content can withstand deformation at high temperatures. Alumina and silica shells are more resistant to swelling in vacuum casting. The high-temperature resistance and chemical durability of the shells play an important role in directional solidification casting [11]. This study examines the use of spent foundry sand in the production of insulating refractory materials. The results indicate that spent foundry sand can be used to create insulation materials with good strength and thermal performance. Analysis shows that the porous materials based on spent foundry sand are environmentally safe [12]. This research developed high-quality ceramic molds for low-pressure turbine blade casting using Ni-based superalloys. The results show that molds with colloidal silica binder (binder B) have lower self-load sag. Meanwhile, ceramic molds with optimized slurry composition (using binder A) produce blade castings with suitable dimensional accuracy and surface roughness [13]. The effects of colloidal silica binders on viscosity, mold strength, self-load sag, shrinkage, and surface roughness of the low-pressure turbine rotor blisks were tested. The investment casting process used BZL12Y superalloy. Ceramic molds were made with mullite and zircon fillers, two types of colloidal silica binders (binder A without polymer and binder B with polymer), and cobalt aluminate solution [14]. This new method was used to create mullite ceramic molds more efficiently. The results showed that these molds have higher strength compared to traditional molds. XRD and SEM analysis helped us understand the structure and grain size of the mullite [15]. Development of $CaZrO_3$ investment molds. Coarse-grained $CaZrO_3$ is used to enhance the durability of the molds, while fine-grained $CaZrO_3$ is employed to improve surface quality. Water-based binders are utilized to maintain corrosion resistance [16]. Investigation of mold systems using silica sol with the addition of needle coke. The research results indicate that the addition of needle coke increases mold thickness, especially at the edges, and sustains higher load capacity. Ceramic molds modified with needle coke show better "green, dry" strength and a lower reduction in "green, wet" strength [17]. This research utilizes low-pressure casting and ultrasonic refinement techniques. This combined process produces samples that are free of gas porosity and solidification defects, improves the microstructure with small α-Al grains, modifies eutectic silicon, and reduces the size of intermetallic phases. The mechanical properties of the alloy are also enhanced [18]. This research discusses methods to maintain ceramic slurry stability in the casting process. The issue of slurry hardening due to air exposure can be addressed by covering the slurry surface with argon gas. After 24 hours, the argon-protected slurry exhibits better viscosity, density, and surface quality than the slurry without argon protection, demonstrating improved stability and mold quality [19]. This study discusses the impact of deflocculants and silicates on the rheology and physico-mechanical properties of ceramic slurry. The addition of silicates has been proven to provide a synergistic effect that improves the rheology and flexural strength of ceramics, with more evenly distributed particles. Overall, these findings are relevant for enhancing the quality of ceramic products in the industry, especially in tile manufacturing [20]. In this process, the application of slurry and stucco (refractory particles) to the wax pattern assembly is repeated, with drying between each successive layer, until a shell mold with sufficient thickness is achieved [21]. In this study, ceramic shells were prepared with several modifications to the conventional slurry. Fine needle coke and coarse needle coke powder were mixed into the inner and outer ceramic slurry layers of the modified ceramic shells [22]. This paper describes the use of Hydroxypropyl methylcellulose as a dispersant to study its effects on the properties of prepared shells and improve the preparation process of fiber-reinforced shells for investment casting [23].

This study explores suspension stability across various parameters. Slurry viscosity increases with albumin content, displaying shear-thickening behavior. Higher viscosity inhibits large aggregate formation, improving wet foam stability during mechanical foaming. Post-sintering results in porous ceramics. Rheological characterization of wet foam includes air content, foam stability, and bubble size distribution [24].

The slurry's rheological behavior is a critical characteristic of powder suspensions used in tape casting. To produce uniform, dense green tapes, the slurry must be well-dispersed, homogeneous, stable, low in viscosity, exhibit shear-thinning behavior, and contain a high solid load. This study investigates the slurry rheology of $CaMgSi_2O_6$ with 4 vol.% Al_2O_3 glass powder, based on preliminary research on its thermal conductivity, as a function of organic additive composition and quantity [25].

This study analyzes how micro- and nano-sized Al_2O_3 particles affect the flow behavior of Mg-Al_2O_3 feedstock in powder injection molding. A binder system with paraffin wax, beeswax, and stearic acid was used. Key parameters like particle size, concentration, and temperature were examined to understand their influence on slurry rheology [26].

This study characterizes the stability of alumina-zirconia-graphite suspensions using rheology, sedimentation tests, and zeta potential measurements with two additives (Glydol and KX9009). These polyelectrolytes have

not yet been explored for graphite powder processing in aqueous systems, though other additives have been studied [27].

This study aims to determine the optimal conditions for preparing stable SiC slurry for slip casting and to correlate its properties with the final ceramic performance. Ammonium polymethacrylate was used as a dispersant, and the effects of its concentration and pH on slurry rheology were analyzed. Optimal dispersion was identified via sedimentation and rheological tests, favoring low viscosity and near-Newtonian flow [28].

Advanced ceramic colloid processing has gained growing attention in high-tech structural materials due to its superior mechanical properties. Rheological measurements are widely used to assess dispersion characteristics, both for fundamental understanding and for evaluating technological suitability. A thorough grasp of dispersion rheology is essential for effective handling. This paper reviews key parameters affecting rheological behavior and the final assessment of colloidal dispersions [29].

This study reveals the microstructure characteristics, slurry rheology, and elemental distribution of ceramic shell molds used in investment casting. The metal casting shell molds discussed in this research are used as examples for casting centrifugal pump impellers.

Experiment

This research was conducted experimentally with the following steps: First, a wax pattern replica was fabricated by injecting wax into an aluminum mold. The molten wax, at a temperature of 80 °C, was injected into the aluminum impeller mold through an injection nozzle at 60-70 °C, with an injection pressure of 10-70 kg/cm². The wax replica produced from the injection process was then removed from the metal mold [1]. Dipping the wax pattern into the ceramic slurry until a ceramic shell mold is formed [13,14,21,30]. The composition of the slurry is shown in Tables 1, 2, 3, and 4, with different compositions for each coating layer. The slurry composition in this study is not significantly different from the compositions used in previous research [4,22, 30,31]. To determine the thickness of the slurry and stucco layers, the wax impeller pattern is dipped into the slurry, and the weight of the slurry and stucco layers adhering to the wax pattern is recorded over time [17]. The wax pattern is dipped into the first slurry/stucco layer, which consists of the materials for Layer I. The first layer is usually a fine layer to ensure a good final casting surface [21], as shown in Table 1.

The wax pattern coated with the first slurry is dried for 24 hours, dried at a temperature of 23-27 °C, for 24 hours. After drying and hardening, and obtained a layer thickness of 0.39 mm, it is then dipped into the second slurry, with the materials shown in Table 2.

The wax pattern, now coated with the second slurry and dried at a temperature of 23-27 °C for 2-4 hours. After drying and hardening, and cumulatively obtained a layer thickness of 1.25 mm, it is then coated with the third slurry, with the materials shown in Table 3.

After being coated with the third slurry and dried at a temperature of 23-27 °C for 2-3 hours. After drying and hardening, and cumulatively obtained a layer thickness of 2.66 mm, and then the wax pattern is coated with the fourth slurry, using the materials shown in Table 4.

After being coated with the 4th slurry and dried at a temperature of 23-27 °C for 2-3 hours. After drying and hardening. Then the thickness of the last layer is measured, and the thickness of the layer is obtained, which is an accumulation of the thickness of the previous layer. And the thickness of the last layer is obtained 3.92 mm.

The viscosity of the slurry affects the process and thickness of the coating against the wax impeller pattern, to maintain the viscosity to remain uniform and stable.

Table 1. Layer 1 slurry material

Colloidal silica, Liter	Wetting agent, cc	Anti Foam, cc	Zircon foam, kg	Sand/ stucco	Viscosity, seconds^{-1}	Drying temperature, °C	Drying time, hours	Coating thickness, mm
9	10	20	40	zircon sand	20-45	23-27	24	0.39

Table 2. Layer 2 slurry material

Colloidal silica, Liter	Zircon flour, kg	Sand/ stucco	Viscosity, seconds^{-1}	Drying temperature, °C	Drying time, hours	Coating thickness, mm
9	40	chamottos 60S	25-35	23-27	2-4	1.25

Table 3. 3-layer slurry material

Colloidal silica, Liter	Mullite (chamttos #200), kg	Sand/ stucco	Viscosity, seconds^{-1}	Drying temperature, °C	Drying time, hours	Coating thickness, mm
12	30	chamottos 35S	25-40	23-27	2-3	2.66

Table 4. 4-layer slurry material

Colloidal silica, Liter	Mullite (chamttos #200), kg	Sand/ stucco	Viscosity, seconds^{-1}	Drying temperature, °C	Drying time, hours	Coating thickness, mm
12	30	chamottos 24S / 22S	25-40	23-27	2-3	3.92

The viscosity of the slurry is determined by a rotating spindle viscometer [28]. In this study, the slurry is stirred continuously [21,30], so that the viscosity of the slurry is maintained at a value between 20-45 s, as shown in Tables 1 to 4. For comparison, it can be seen in previous research [23,28].

The kinetics of slurry hardening are studied by measuring variations in slurry viscosity over time [32].

Most water-based primary coatings consist of colloidal silica binders combined with suitable ceramic fillers. Compared to alcohol-based variants, water-based silica binders dry more slowly—an advantage that allows ample time for manipulation during the plastering (stuccoing) stage to ensure a smooth, even layer and thorough surface coverage [21].

To strengthen the mechanical bond between the coating particles, different layers of sand sizes are used, and the finer the sand particle size, the finer the stucco layer of the mold shell cavity surface.

Coatings 5 through 7 are applied using the same slurry materials and methods, with a layer thickness of 5.19 mm, 7.13 mm, and 9.94 mm, which is the average value. Measurement of layer thickness on the 4th dyeing, 5, 6, 7 shown in Fig. 1. Fig. 2 shows an example of the shape of the slurry and stucco coating result. The wax pattern is dipped in the slurry liquid (Fig. 2(a)) and the stucco (Fig. 2(b)). This process is repeated until a layer of shell ceramics with a thickness of 9-10.5 mm is obtained. The shell ceramics are dried at a room temperature of 23-27 °C to form a mold.

Depending on the required cooling rate and subsequent metallurgical properties, the shell typically consists of five to eight layers [21]. The slurry adheres to the wax pattern by gravity, without applying pressure. The slurry is continuously stirred with a stirrer. The slurry that adheres to and is retained on the wax pattern can be seen as a total thickness consisting of many very thin layers [17].

The evaporation of wax from the ceramic shell using boiler steam leaves a hollow space or cavity that retains the shape of the wax pattern. The melting and evaporation of the wax are carried out in an autoclave. The process of melting the wax pattern for creating ceramic molds in investment casting generally occurs at relatively low temperatures, ranging from 65 to 80 °C. At this temperature, the wax becomes liquid and can be easily removed from the mold, leaving a shell cavity that

Fig. 2. Example of coating: a) Coating slurry to wax pattern, b) Coating stucco

Fig. 1. Measurement of layer thickness, a) 4th layer; b) the 5th layer; c) the 6th layer; d) 7th layer

Fig. 3. Ceramic shell after de-waxing.

matches the shape of the wax pattern. An example of a ceramic shell after wax evaporation is shown in Fig. 3.

Sintering the ceramic shell mold hardens the ceramic material. The sintering process aims to produce a hard ceramic shell that is resistant to heat, pressure, and high temperatures during metal casting. The sintering temperature for the ceramic shell in this investment casting study was set at 1050 °C. This temperature was applied after the wax pattern was melted.

The removal of wax from the mold is carried out by burning it up to a temperature of 1000 °C

to achieve maximum ceramic bonding [21]. Scanning electron microscopy (SEM) analysis shows that the mullitization behavior is influenced by the sintering temperature [15]. Solid-phase sintering transforms bulk powder from discrete microscopic particles into a continuous solid-state structure through material diffusion at high temperatures. Consequently, the overall surface energy in the system decreases, while the sample density and strength increase [15].

For SEM-EDX testing, ceramic shell samples were cut according to the SEM-EDX test sample requirements, measuring 10 × 10 × 5 mm. The SEM EDX test results for each sintering temperature were analysed for the distribution of elements contained in the ceramic shells.

Scanning electron microscopy (SEM) was used to examine the microstructure of the inner and outer surfaces of the ceramic shells [22].

Results and Discussion

SEM EDX testing is conducted to identify the microstructure, porosity cavities, and slurry rheology conditions within the ceramic shells used in investment casting. EDX testing determines the distribution of elements contained within the ceramic shell material. The porosity cavities formed in the ceramic shells will affect the shell's resistance to the impact of molten metal when it is poured. However, in this study, no mechanical properties test, especially impact test, was carried out, because the liquid metal pouring process is suspected to have not too much impact on the mold wall.

Figure 4 illustrates the microstructure of the ceramic shell used in investment casting. In this study, the ceramic shell was sintered at 1050 °C. The figure shows the microstructure of stucco sand grains with interfacial bonds. It demonstrates that the interfacial bonds between the sand grain aggregates occur mechanically. The stucco sand grains in the figure have particle sizes of less than 100 μm, and the irregular surface of the sand grains aids in mechanical interfacial bonding between the grains, forming agglomerations to create the ceramic shell for investment casting.

In this study, the aggregates in the shell mold are stucco sand and mullite, with colloidal silica used as the inorganic binder in the shell mold. Fig. 4 also shows porosity cavities, cracks, and gaps between the aggregates. These porosity cavities, cracks, and gaps have the potential to become gas traps formed by the flow of molten metal when poured. The porosity cavities that appear on the surface of the mold cavity will affect the smoothness of the surface of the metal product in investment casting. The features of colloidal silica in the image are identified as the rheological properties of the slurry. These features show that the colloidal silica exhibits mechanical adhesion and bonding between the aggregates, with irregular surface shapes. Maintaining the rheological properties of the primary slurry is crucial because it directly contacts the mold pattern. The slurry's rheology is monitored and adjusted by adding deionized water as evaporation occurs.

The primary issue with ceramic slurry in casting is hardening when exposed to air, which shortens its shelf life. The quality of the mold depends on the stability of the slurry's rheology. This study focuses on maintaining the consistency of the primary slurry,

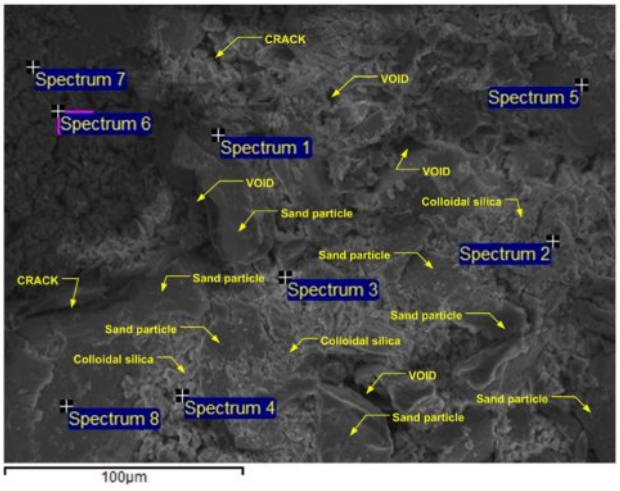

Fig. 4. Points of EDS test spectrum of ceramic sintered 1050 °C.

which is prepared in an open steel container [19]. To prevent the thickening and premature hardening of the slurry, it is continuously stirred. The rheology of the slurry refers to the physical properties of this mixture, such as viscosity, thickness, and stability. A slurry with good rheology will be easy to apply and will form a consistent layer free from unwanted pores [21,30]. The production of high-performance components is influenced by the control of the microstructure [10]. The microstructure of ceramics is affected by the rheological properties of the slurry during pressure-free immersion. The microstructure of the pores formed on the outer and inner surfaces of sintered mullite is primarily investigated using scanning electron microscopy (SEM) [9,21]. The phase composition and microstructure are fundamental characteristics that determine the performance of porous insulating refractories [12]. The mechanism of pore generation in the sample can be summarized as powder combustion, particle agglomeration, and in situ reactions [12]. During the sintering process, the green shell mold undergoes interesting changes. Initially, there are many individual grains with large surface areas and pores. However, during sintering, the crystal grains grow, and the surface energy decreases, leading to pore shrinkage. Eventually, the pore network stabilizes, and densification of the sample occurs after the release of the pores [15]. The microstructure investigated by SEM is characterized by good bonding of the coating and stucco layers, and a porous matrix resulting from coarse grains packed in a fine-grained network. The use of fine-grained slip for the first layer significantly improves the quality of the internal surface [16]. This slurry acts as a binder containing silica sol, which helps ceramic particles stick together and form larger agglomerates, ensuring that the particles are evenly distributed and strongly bonded. The consistency of the slurry is adjusted to ensure the proper viscosity, allowing small particles to easily merge into larger aggregates. Proper viscosity helps maintain the uniformity of the slurry layer on the mold. A wetting agent in the slurry helps reduce surface tension, allowing particles to move closer together and form aggregates more effectively. When the slurry is applied to the wax pattern and allowed to dry, the ceramic particles settle and bond with each other, forming a strong and solid structure. This drying process also aids in the integration of the particles. The multi-layered ceramic shell is sintered at high temperatures, in this study at 1050 °C, to strengthen the particle agglomeration through the fusion of ceramic particles [21,22,23,30].

The following equations are used to determine the rheological properties of the slurry. These equations measure the viscosity and flow of non-Newtonian fluids.

Newton's Law:

For Newtonian fluids [23,33], viscosity (η) is constant and flow can be explained by the equation:

$$\tau = \eta \times \dot{\gamma} \quad (1)$$

Catatan: t = shear stress [N/m²]
h = Viscosity[N·s/m²]
$\dot{\gamma}$ = shear rate [s⁻¹]

Model Bingham Plastic: Used for fluids that require an initial shear stress to start flowing [33].

$$\tau = \tau_0 + \eta_p \times \dot{\gamma} \quad (2)$$

Catatan: t_0 = Initial shear stress [N/m²]
h_p= Plastic Viscosity [N·s/m²]
$\dot{\gamma}$ = shear rate [s⁻¹]

Model Power Law: For pseudoplastic or dilatant liquids, the viscosity changes with the shear rate [34].

$$\tau = K \times \dot{\gamma}^n \quad (3)$$

Catatan: τ = shear stress [N/m²]
K = Index consistency [Pa]
$\dot{\gamma}$ = shear rate [s⁻¹]
n = The flow index is a dimensionless number (has no units)

light (dilute) shear fluid if n < 1, and heavy (viscous) shear fluid if n >1 [33].

Model Herschel-Bulkley: The Combination of Bingham Plastic and Power Law [35].

$$\tau = \tau_0 + K \times \dot{\gamma}^n \quad (4)$$

Equations (1), (2), (3), and (4) indicate that the rheological properties of the slurry in the formation of the ceramic shell are influenced by the viscosity of the slurry as it flows between the reinforcing aggregates of the mold. Other factors affecting rheological properties include the shear rate of the slurry as it flows between the gaps of the aggregates and the surface roughness of the aggregate grains. The viscosity and shear rate of the slurry affect the shear stress of the slurry fluid. In this research, the slurry flow is not applied with forced pressure but relies on the dipping depth pressure.

Figure 5 explains the distribution map of elements contained in the ceramic shell of the investment casting mold after sintering at 1050 °C. The mixed map shows that the silica content is unevenly distributed over large, separated areas. Oxygen content is also unevenly distributed, represented in green, across numerous separated areas. Aluminum is also present in the mixed

The map in blue shows an uneven, separated distribution. The mapping in Fig. 5 is based on elemental testing at spectrum points 1 through 8, as shown in Fig. 4.

This figure displays nine panels, each labeled with different chemical elements and colors. Here is a more detailed explanation:

"Mixture" in this context refers to the combination or mixture of several elements or components. In the image, areas labeled as "Mixture" may indicate regions where multiple elements are present simultaneously or mixed.

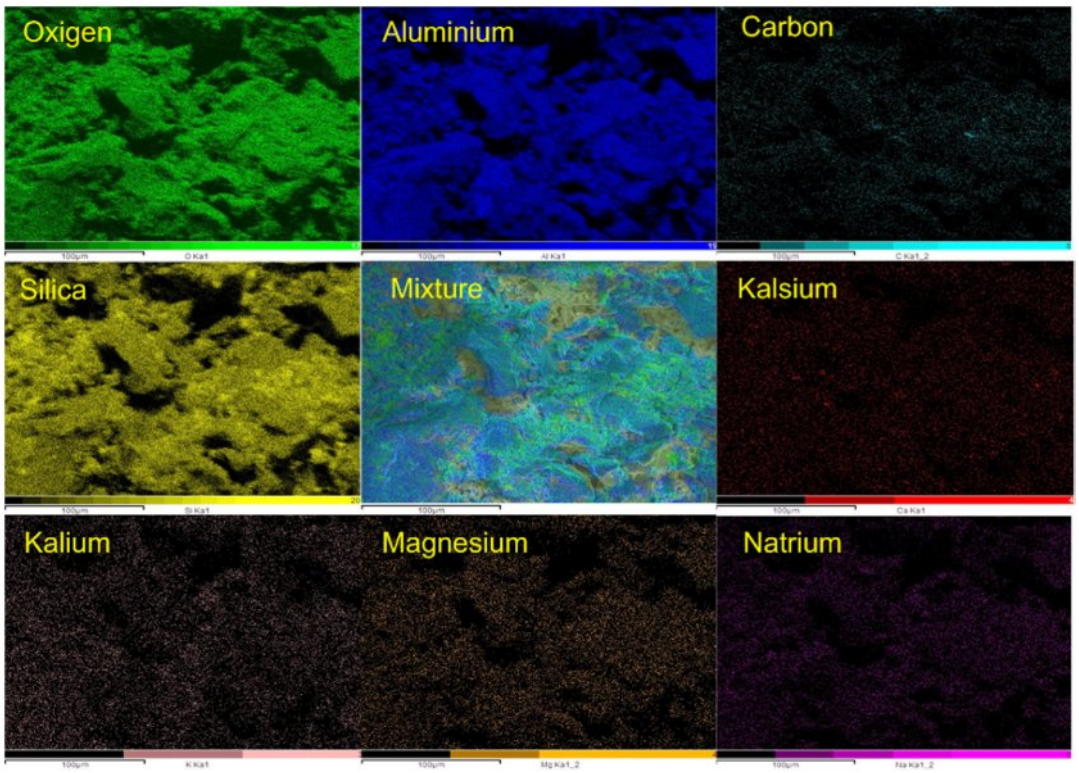

Fig. 5. Elements dispersal map of ceramic sintered at 1050 °C.

The weight percentage content of each element is shown in Table 5. All spectrum points indicate that the element with the highest weight percentage is oxygen, with an average content of 56.11% by weight. The silica content shows a weight percentage of 20.91%. Aluminum content is 13% by weight, and carbon is 9.10% by weight. All element contents in the ceramic shells sintered at 1050 °C are shown in Table 5. These elements are C, O, Na, Al, Si, Ti, K, and Mg. Not all spectrum points show the same element content, indicating that the distribution of elements is unlikely to be uniform.

The main components of the ceramic slurry used in the investment casting process result in the highest oxygen content, as determined by the EDS (Energy Dispersive X-ray Spectrometry) test, after sintering the ceramic mold at 1050 °C. The ceramic slurry consists of refractory powders such as zircon, silica, and aluminosilicates, all of which contain high levels of oxygen. Oxygen is a primary element in these refractory materials, and during high-temperature sintering, the oxide structure remains intact, becoming a major component of the ceramic mold. Therefore, when EDS analysis is performed, the oxygen element will show high intensity compared to other elements [4,19,22,30,31].

The second highest element is silica. This is normal

Table 5. Elements of ceramic investment casting sintered at 1050 °C

	Elements, % weight.										
Spectrum points	C	O	Na	Al	Si	Ti	K	Mg	Fe	Ca	sum
1	6.71	55.45	0.23	15.86	21.45	0.31	0	0	-	-	100.01
2	7.84	59.58	0.4	9.79	21.96	0.2	0.22	0	-	-	99.99
3	9.15	62.5	0.45	5.49	22.12	0.08	0.22	0	-	-	100.01
4	7.41	58.85	0.59	12.24	20.26	0.23	0.42	0	-	-	100
5	11.28	52.75	0.29	16.78	18.09	0	0.8	0.01	-	-	100
6	7.74	56.22	0.29	12.78	22.47	0.33	0.17	0	-	-	100
7	17.06	52.42	0	13.95	16.57	0	0	0	-	-	100
8	5.64	51.11	0.53	17.27	24.34	0.48	0.64	0	-	-	100.01
Average	9.10	56.11	0.35	13.02	20.91	0.20	0.31	0.00	-	-	100.00

because the slurry material for the ceramic shell mold is silica.

Conclusion

Research and observation of the rheological properties of the ceramic shell mold slurry for investment casting have been conducted. The irregular surface of the sand grains aids in mechanical interfacial bonding between the grains, forming agglomerations to create the ceramic shell for investment casting. The aggregates in this shell mold study are stucco sand and mullite, with colloidal silica used as the inorganic binder in the shell mold.

The features of colloidal silica in the image are identified as the rheological flow properties of the slurry after the sintering process. These features show that the colloidal silica exhibits mechanical adhesion and bonding between the aggregates, with irregular surface shapes. The slurry acts as a binding medium to form agglomerations of the particles that make up the ceramic shell mold.

The rheological properties of the slurry in forming the ceramic shell are influenced by the viscosity of the slurry and the shear rate of the slurry as it flows between the aggregates, taking into account the surface roughness of the reinforcing grains. The viscosity and shear rate of the slurry affect the shear stress of the slurry fluid, which relies only on the dipping depth pressure. Oxygen is the highest element in the ceramic shell after the ceramic shell is sintered at a temperature of 1050 °C. The oxygen content reaches 56.11%; silica 20.91%; aluminium 13.02%, and carbon 9.10%.

Acknowledgments

The author is grateful to PT. Trieka Aimex provides facilities to carry out this research.

The author thanks the Research and Community Service Unit of Politeknik Negeri Jakarta. The authors acknowledge the facilities, scientific and technical support from Advanced Characterization Laboratories Serpong, National Research and Innovation Agency through E-Layanan Sains, Badan Riset dan Inovasi Nasional (BRIN).

References

1. A. Dermawan and A.E. Pramono,Recent Eng. Sci. Technol. [01] (2023) 11-19.
2. Q. Liu, M.C. Leu, and V.L.R. Stephen, Int. J. Adv. Manuf. Technol. [24] (2004) 485-495.
3. V.K. Tiwary, P. Arunkumar, A.S. Deshpande, and N. Rangaswamy, Rapid Prototyp. J. [5] (2019) 904-914.
4. S. Pattnaik, Int. J. Adv. Manuf. Technol. [93] (2017) 691-707.
5. V. Lopes, H. Puga, I. . Gomes, N. Peixinho, J.C. Teixeira, and J. Barbosa, J. Mater. Process. Technol. 299 (2022) 117339.
6. K. Lee, S. Blackburn, and S.T. Welch, J. Mater. Process. Technol. [225] (2015) 369-374.
7. S. Amira, D. Dubé, and R. Tremblay, J. Mater. Process. Technol. [211] (2011) 1336-1340.
8. D. Liao, Z. Fan, W. Jiang, E. Shen, and D. Liu, J. Mater. Process. Technol. [211] (2011) 1465-1470.
9. W. Singhapong, P. Srinophakun, and A. Jaroenworaluck, J. Aust. Ceram. Soc. [53] (2017) 811-820.
10. Y. Zhu, D. Luo, Z. Li, Y. Wang, H. Cheng, F. Wang, and T. Chen, J. Alloys Compd. 820 (2020) 153153.
11. Y. Venkat, N. Hazari, M.A.H. Baig, S. Singh, and N. Das, Int. J. Cast Met. Res. [26] (2013) 114-121.
12. R. Xiang, Y. Li, S. Li, Z. Xue, and L. Yuan, J. Aust. Ceram. Soc. [57] (2021) 427-433.
13. Y. Venkat, K.R. Choudary, D.K. Das, A.K. Pandey, and S. Singh, Ceram. Int. [46] (2020) 26572-26580.
14. Y. Venkat, K.R. Choudary, D.K. Das, A.K. Pandey, and S. Singh, Ceram. Int. [47] (2021) 5663-5670.
15. Q. Wei, J. Zhong, Z. Xu, Q. Xu, and B. Liu, Ceram. Int. [44] (2018) 12088-12097.
16. L. Freitag, S. Schaffoner, N. Lippert, C. Faßauer, C.G. Aneziris, C. Legner, and U.E. Klotz, Ceram. Int. 43[9] (2017) 6807-6814.
17. F. Wang, F. Li, B. He, and B. Sun, Ceram. Int. [40] (2014) 479-486.
18. J. Barbosa and H. Puga, J. Mater. Process. Technol. [244] (2017) 150-156.
19. S. Pattnaik and M.K. Sutar, Arab. J. Sci. Eng. [46] (2021) 12065-12076.
20. N. Ercioglu Akdogan, E. Arioz, and O.M. Kockar, J. Dispers. Sci. Technol. [46] (2023) 119-129.
21. B.S. Sidhu, P. Kumar, and B.K. Mishra, J. Mater. Eng. Perform. [17] (2008) 489-498.
22. S. Kumar and D.B. Karunakar, Int. J. Met. [15] (2021) 98-107.
23. K. Lü, Z. Duan, X. Liu, Y. Li, and Z. Du, Int. J. Met. [14] (2020) 1005-1012.
24. W.Y. Jang, B. Basnet, J.G. Park, H.M. Lim, T.Y. Lim, and I.J. Kim, J. Ceram. Process. Res. 19[4] (2018) 296-301.
25. G.N. Sun and E.S. Kim, J. Ceram. Process. Res. [13] (2012) 346-350.
26. S.M. Taheri, E. Ghasemi, M. Alizadeh, and R.Y. Rad, J. Ceram. Process. Res. [15] (2014) 236-241.
27. H. Majidian and T. Ebadzadeh, J. Ceram. Process. Res. [16] (2015) 298-302.
28. N.V. Lakshmi, A. Dey, N. Kayal, and O. Chakrabarti, J. Ceram. Process. Res. [15] (2014) 97-101.
29. D. Sharma and A. Mukherjee, J. Ceram. Process. Res. [16] (2015) 690-704.
30. S.N. Bansode, V.M. Phalle, and S.S. Mantha, Trans Indian Inst Met [73] (2020) 763-773.
31. Z. Li, X. Liu, Y. Lu, and K. Lv, J. Adhes. Sci. Technol. [36] (2022) 469-489.
32. Q. Liu, V.L. Richards, K.P. Daut, and M.C. Leu, Int. J. Cast Met. Res. [19] (2006) 195-200.
33. K.R. Mrinal, M.H. Siddique, and A. Samad, Part. Sci. Technol. [36] (2018) 38-45.
34. G.A. Campbell, M.E. Zak, and M.D. Wetzel, Rheol. Acta [57] (2018) 197-216.
35. Z. Wang, S. Wu, Y. Liu, J. Zhang, Y. Chen, Z. Qin, J. Su, C. Sun, and H. You, Appl. Sci. 13[5] (2023) 2802.